Boosting solar cell photovoltage via nanophotonic engineering

Y. Cui[1#], D. van Dam[*1#], S.A. Mann[2], N.J.J. van Hoof[1], P.J. van Veldhoven[1], E.C. Garnett[2], E.P.A.M. Bakkers[1,3], J.E.M. Haverkort[2]

[#] equal contribution

[1]Applied Physics, Eindhoven University of Technology, PO Box 513, 5600 MB Eindhoven, The Netherlands.

[2]Center for Nanophotonics, FOM Institute AMOLF, Amsterdam, The Netherlands.

[3]Kavli Institute of Nanoscience, Delft University of Technology, The Netherlands.

[*]Correspondence to: a.d.v.dam@tue.nl

Approaching the theoretically limiting open circuit voltage (V_{oc}) of solar cells is crucial to optimize their photovoltaic performance. Here we demonstrate experimentally that nanostructured layers can achieve a fundamentally larger Fermi-level splitting, and thus a larger V_{oc}, than planar layers. By etching tapered nanowires from planar InP, we directly compare planar and nanophotonic geometries with the exact same material quality. We show that the external radiative efficiency of the nanostructured layer at 1 sun is increased by a factor 14 compared to the planar layer, leading to a 70 mV enhancement in V_{oc}. The higher voltage arises from both the enhanced outcoupling of photons, which promotes radiative recombination, and the lower active material volume, which reduces bulk recombination. These effects are generic and promise to enhance the efficiency of current record planar solar cells made from other materials as well.

To maximize the conversion efficiency of sunlight into electricity, a photovoltaic device needs to simultaneously achieve optimal photocurrent and voltage. Nanophotonic engineering has been employed to enhance the photocurrent of solar cells by reducing reflection and increasing solar light absorption via light trapping[1–7], and values close to full absorption have already been achieved[8]. Therefore, in order to bring the photovoltaic conversion efficiency closer to the theoretical limit as determined by Shockley and Queisser[9], the open circuit voltage (V_{oc}) needs to be further improved[10–13].

The V_{oc} is generally expressed as a function of photocurrent density J_{sc} and dark current density J_0 as $V_{oc} \approx \frac{k_B T}{q} \ln \frac{J_{sc}}{J_0}$, in which k_B, T and q are the Boltzmann constant, solar cell temperature, and electron charge, respectively[14].

The dark (saturation) current density is proportional to the recombination rate, and can be separated into a radiative part and a non-radiative part. Maximizing the voltage requires minimizing recombination, but even a perfect solar cell must undergo radiative recombination to remain in thermal equilibrium with its surroundings. As such, radiative recombination is not a loss but a thermodynamic necessity, and optimizing external light emission therefore improves solar cell performance[15]. On the other hand, *non*-radiative recombination caused by bulk defect and surface recombination, constitutes a loss that can be eliminated. Therefore, improving the V_{oc} requires increasing the ratio of external radiative to total recombination rates, which is equivalent to increasing the external radiative efficiency (η_{ext}). This fact implies that optimization of a solar cell's power output requires not only maximizing the internal radiative efficiency (η_{int}), which gives the fraction of internal recombination events that is radiative, but also requires optimizing the average escape probability of an internally emitted photon ($\overline{P_{esc}}$). This counterintuitive phenomenon is explained in more detail elsewhere[15–17] and in the Supplementary Information. Bulk (Shockley-Read-Hall) non-radiative recombination in a solar cell is proportional to the amount of active material, which means that η_{int} can be improved by reducing the amount of material[18] if surface recombination plays a minor role. Additionally, efficient outcoupling of internally emitted photons is essential, because it prevents eventual non-radiative recombination due to photon reabsorption[15]. Therefore, reducing the amount of absorber material and enhancing $\overline{P_{esc}}$ of emitted photons can improve the V_{oc}. This becomes directly apparent from the equation for the V_{oc} (valid for $\eta_{int} < \sim 0.1$):

$$V_{oc} = V_{oc}^{rad} - \frac{k_B T}{q} |\ln \eta_{int} \overline{P_{esc}}| \quad \text{(Eq1)}$$

where V_{oc}^{rad} is the V_{oc} in the radiative limit (in absence of non-radiative recombination, see derivation in Supplementary Information). This shows that improvements in η_{int} and $\overline{P_{esc}}$ are equally important

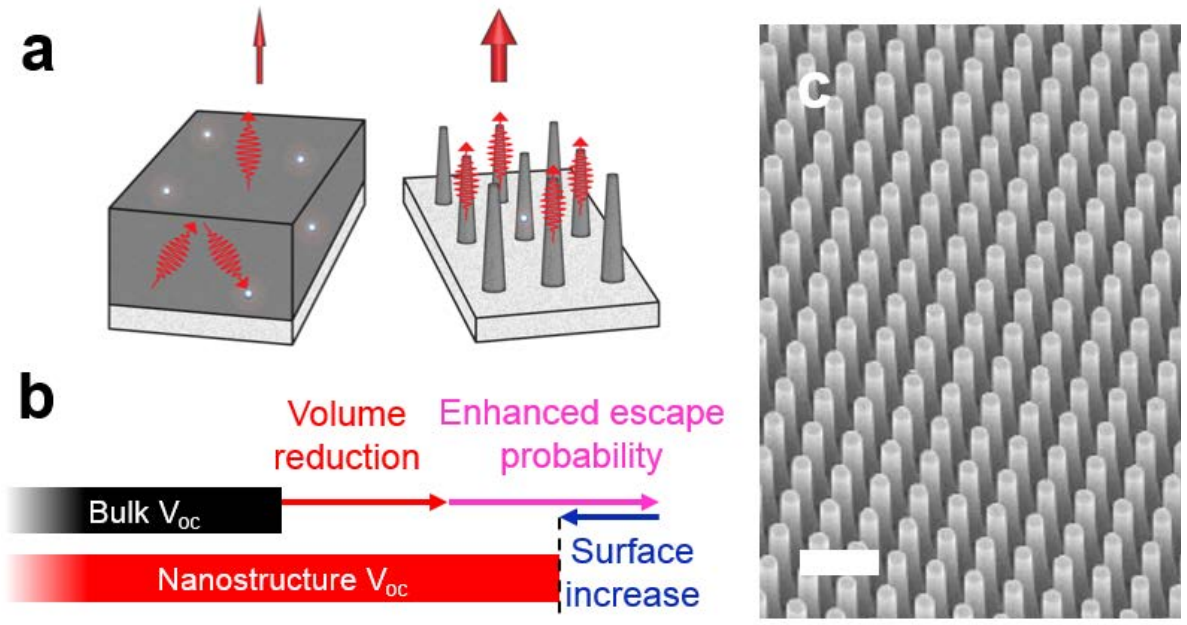

Fig. 1. Effect of nanowire geometry on V_{oc}. a) A planar InP sample is compared with a piece of the same material in which a nanowire structure is defined by etching: the emission outcoupling enhanced and the number of bulk defect is reduced. b) Schematic of the effects of the nanostructuring on the V_{oc}. Because of reduced bulk recombination and enhanced outcoupling, the emission intensity (red upward arrow) is enhanced, indicating a higher V_{oc}. c) Scanning Electron Micrograph of the etched nanowire array, imaged at a 30 degree tilt. The scale bar represents 1 micron.

for increasing the V_{oc}. For improving η_{int} by reducing material volume, we need to make sure to simultaneously maintain maximum absorption of sunlight. This can be achieved using the antenna effect of nanostructures, which allows them to absorb light from a larger area than their projected geometrical area[3,13,19]. For minimizing losses due to the $\overline{P_{esc}}$ term, enhanced outcoupling of internally generated photons can be achieved in tapered nanowires by utilizing adiabatic expansion of the optical mode confined in the nanowire into free space[20]. The two described mechanisms, applied to tapered nanowires, are schematically displayed in Figure 1a. Figure 1b shows the effects on the V_{oc}, including a possible reduction due to the increased surface area. A high V_{oc} in a nanostructured solar cell has been reported recently[21], but it could not be directly compared to the planar geometry because of the nanowire's crystal structure and the growth mechanism which is different from that of planar layers.

Here we demonstrate that nanostructuring enhances the V_{oc} of the exactly identical material in planar morphology, due to the two mechanisms described above.

To investigate the effect of nanostructuring on the V_{oc}, we compare planar indium phosphide (InP) material with a piece from the same sample in which we have defined nanostructures by top-down lithographic techniques. The planar and nanostructured samples thus consist of identical material from the same growth run, which allows us to isolate the effect of nanostructuring on the V_{oc}. We use an intrinsic epitaxial InP layer of 1600 nm grown by metal-organic vapour-phase epitaxy (MOVPE), on top of an InP wafer. We chose InP because it has a direct band gap with the ideal energy for photovoltaic devices (E_g=1.34 eV), and a low surface recombination velocity[22]. The nanostructured sample (a periodic array of conically shaped nanowires) is fabricated by selectively dry etching the thin film through a chromium mask patterned by nanoimprint lithography, followed by digital etching to remove surface defects (more information in the Method section). The result is shown in a scanning electron micrograph in Figure 1c. The period of our square array is 513 nm, where the 1.6 micron long tapered wires have a base diameter of 350 nm and a top diameter of 150 nm. The conical shape is chosen because of its very high absorptance[6,19,23], which for InP can be over 98% in the full wavelength range between 400 and 900 nm[19].

To compare the V_{oc} with and without nanostructuring, we use the fact that the photoluminescence (PL) emission intensity in a semiconductor is directly related to the splitting of its quasi-Fermi levels[24–27] (see Supplementary Information). We can therefore use calibrated PL measurements as a contactless probe for the V_{oc}. PL emission spectra of InP with and without nanostructuring are shown in Figures 2a (absolute counts) and 2b (normalized counts), measured at room temperature. The normalized emission spectra are identical and only show band gap related emission, but the nanowire layer shows a 20-fold higher emission intensity. This increased emission cannot be explained by the increase in absorptance alone, which only accounts for a factor of 1.4 (see Supplementary Information). Power dependent PL emission intensities are shown in Figure 2c (more information in Method section and Supplementary Information). The number of suns corresponding to the incident photon intensity is plotted on the top horizontal axis. From the absorbed and emitted photon

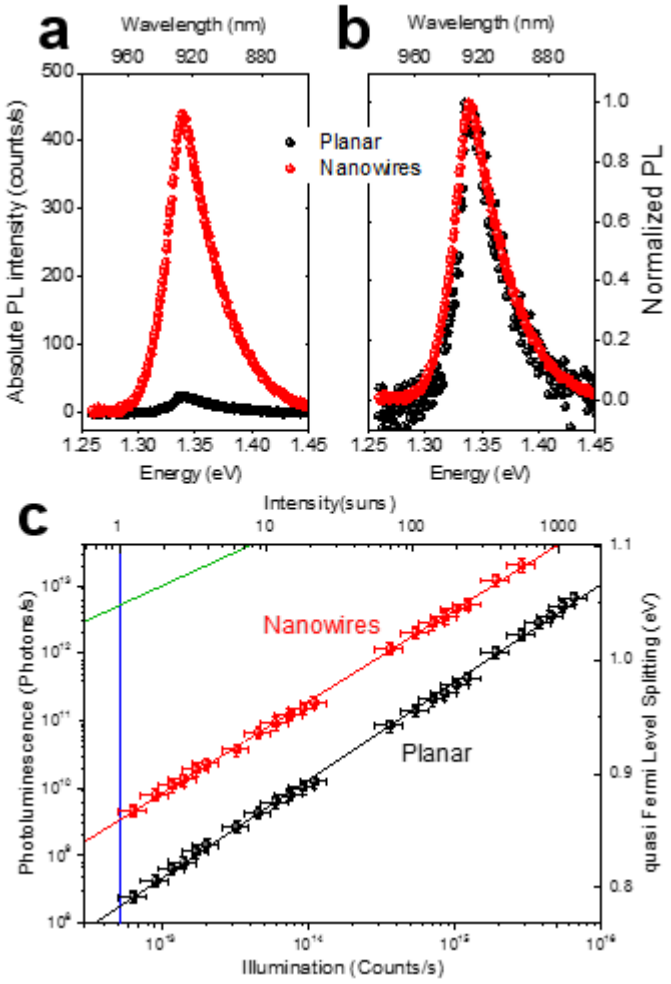

Fig. 2. Determination of quasi-Fermi level splitting by photoluminescence. Photoluminescence spectra of a) planar layer (black) and nanowire layer (red). b) same as A, but normalized to their respective maxima, to allow comparison of the shapes. c) Power-dependent PL for planar (black) and nanostructured (red) InP films, corrected for absorption at the PL wavelength. The illumination intensity is converted into suns (top axis) and the PL intensity is expressed as Fermi level splitting (right axis). The blue line corresponds to 1 sun and the green line is the ideal curve for a sample with external radiative efficiency equal to 1. The red and black curves are linear fits through the data.

intensities at 1 sun, we calculate η_{ext} = (7.0±0.9)*10^{-4} for the nanowire array and (5.2±0.5)*10^{-5} for the planar sample. The quasi-Fermi level splitting (equivalent to the maximum achievable V_{oc} in a contacted device) obtained from the integrated PL intensity is displayed on the right axis (full justification in Supplementary Information). It is clear that nanostructuring increases the Fermi level splitting compared to the planar film for the entire excitation intensity range from 1 to 1000 suns. At 1 sun the

implied V_{oc} is 70 mV higher for the nanostructured sample compared to the planar sample, demonstrating that a nanostructured solar cell allows an intrinsic advantage in photovoltage over a planar layer.

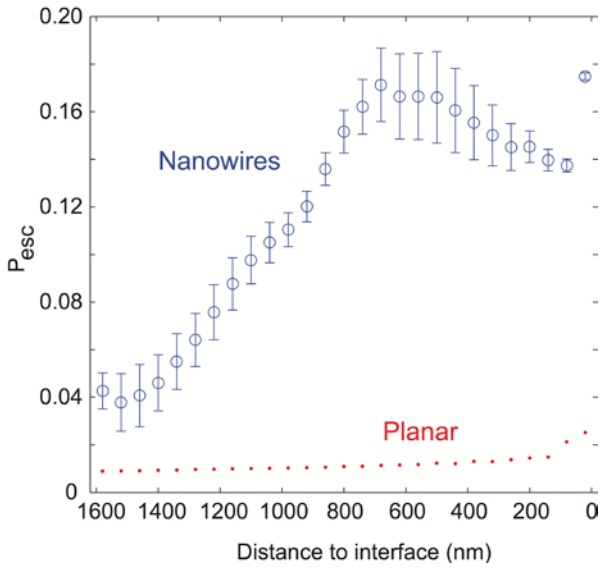

Fig. 3. Photon escape probability for nanowires and planar. Simulated photon escape probability as a function of the distance to the nanowire-layer-air or InP-air interface.

The enhancement of the V_{oc} stems from a number of different contributions, as depicted schematically in Figure 1b. The first contribution is the reduction of material volume by a factor of 5.1, which therefore also reduces the non-radiative bulk recombination rate by the same factor as the radiative recombination rate is proportional to the number of bulk defect centers. If the total non-radiative recombination is dominated by bulk recombination (see Supplementary Information), this would result in an increase in V_{oc} of 42 mV. We emphasize that due to the optical antenna effect of the nanowires, the reduction in material volume does not decrease the short circuit current, as we will also discuss later. The second contribution to the improved V_{oc} is enhanced light outcoupling. We have simulated the photon escape probabilities P_{esc} for randomly oriented dipoles inside the absorption region of the material, shown in Figure 3, both for nanowire layers and planar layers. We found average photon escape probabilities of 2.1% and 13% for the planar and nanowire samples, respectively (more

details in Supplementary Information, section 5), leading to an enhancement factor of 6.3. For materials with a low internal luminescence efficiency (<10%), this enhanced escape probability corresponds to an increase in V_{oc} of 47 mV. Since these effects together would result in a larger increase of V_{oc} (89 mV) than we have observed, we argue that increased surface recombination due to the increased surface area for the nanowires sample partially compensates the gain in V_{oc}. These results show, however, that even without additional surface passivation steps, the net V_{oc} is enhanced by nanostructuring. If we assume an average photon escape probability from the nanowire layer of 13%, we derive an $\eta_{int} \approx 0.54$ % at 1 sun (comparison in Supplementary Information). We note that while a much higher η_{int} has been reported for n-doped GaAs[28], heavily n-doped InP[29] and InP micropillars[27], we are not aware of such high η_{int} for the p-doped case[30].

We emphasize that the V_{oc} enhancement is not a "concentration" effect, since light concentration changes the entropy between incident and emitted photons, and thus modifies the thermodynamic limit given by V_{oc}^{rad}. Such a thermodynamic enhancement is in principle possible using nanowire arrays, but requires a specifically engineered angular emission profile[31], which is outside the scope of the present paper. Furthermore, we have checked the angular profiles of our nanostructured and planar samples, and they are not significantly different (Supplementary Figure S6). Finally, the enhanced V_{oc} is not caused by effective band gap modification due to nanophotonic resonances[11] or different crystal structures, as we can learn from the energy of the emitted PL. Based on these arguments we can conclude that the V_{oc} enhancement can only be due to an effective volume reduction and an enhanced photon escape probability.

Finally, to explore the general effect of nanostructuring on the V_{oc}, we have used the more general form of equation (1), $V_{oc} = V_{oc}^{rad} - \frac{k_B T}{q}\left|\ln\frac{\eta_{int}\,\overline{P_{esc}}}{1-\eta_{int}(1-\overline{P_{esc}})}\right|$ (valid for any η_{int}, as long as there is no parasitic absorption), to investigate the potential for further improvement of present day solar cells by nanostructuring. In Figures 4a&b we have expressed the maximum V_{oc} (for InP) as a function of the photon escape probability and the material filling fraction f, for two different values of η_{int}. The full equations are listed in the Supplementary Information. We observe a clear logarithmic dependence of the maximum V_{oc} on $\overline{P_{esc}}$ and on f for the low internal luminescence efficiency. However, even layers

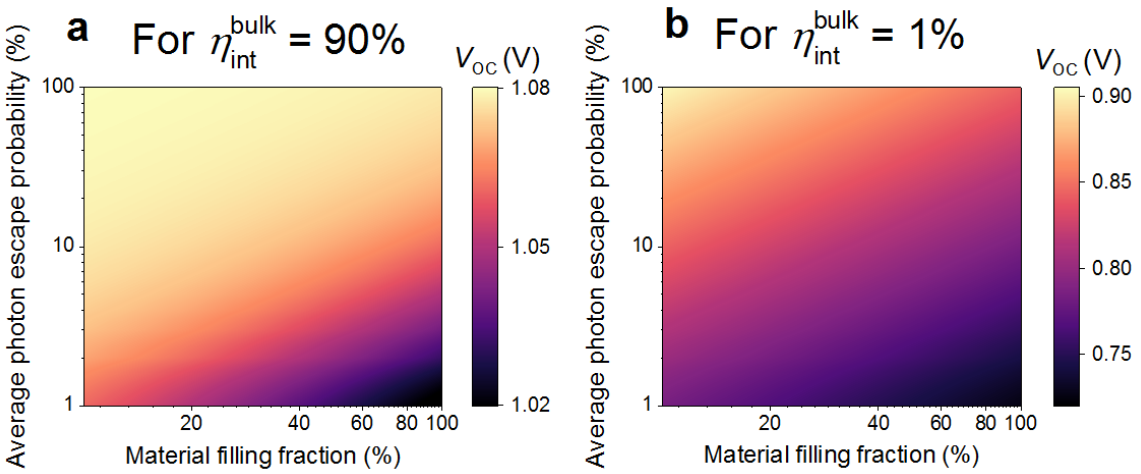

Fig. 4. Enhancement of solar cell V_{oc} as a function of photon escape probability and material filling fraction. (a, b) Calculated V_{oc} values for InP cells expressed in a log-log plot, as a function of the photon escape probability and the material filling fraction, for a fixed internal radiative efficiency of 90% (a) and 1% (b).

with 90% internal luminescence efficiency can still gain tens of millivolts by improved photon escape probability and material volume reduction. Of course, the advantage vanishes when η_{int} approaches 1 very closely. Note that the choice of semiconductor defines only the value of the V_{oc} in the radiative limit, and has no influence on the loss terms related to f and $\overline{P_{esc}}$, which makes these effects generic for all solar cell materials as long as surfaces are well passivated. Figure 4 assumes that the surface recombination rate is small compared to the bulk recombination rate, while some materials instead suffer from high surface recombination velocities. However, for solar cell materials such as silicon[32,33] and GaAs[34,35] it has already been shown that surface recombination can be greatly reduced by proper surface passivation. This is required to utilize nanostructured solar cells made of these materials.

For optimal solar cell performance, not only V_{oc} but also J_{sc} needs to be close to the theoretical maximum. As we have shown above, a reduction of material can substantially enhance light absorption, and we note that the volume can be reduced to a at least a factor f~0.08 in (nano)wire arrays without losing any absorption with respect to a planar layer, as has been demonstrated for materials such as silicon, InP and GaAs[19,36,37]. This makes the relative increase in V_{oc} in Figure 4 also indicative for the relative increase in cell efficiency. From Figure 4 we can derive the optimum design requirements for

153 new record high-V_{oc} solar cells: starting from a high internal radiative efficiency solar cell material, a
154 very high photon escape probability should be combined with a very small amount of material. We
155 finally conclude that nanostructuring is a very effective approach to increase both the solar cell
156 photovoltage and the photocurrent to approach the Shockley-Queisser limit.

Methods

Nanowire array fabrication. The fabrication of our top-down etched nanowire array starts with MOVPE growth of an intrinsic InP layer on a Zn doped InP (100) substrate at a temperature of 650 °C. An array of chromium nano-discs is patterned by nanoimprint lithography. Subsequently, the Cr nano-disc pattern is transferred an array of SiN_x nano-cylinders by RIE etching. These SiN_x nano-cylinders will serve as a hard-mask for 40 min ICP etching at 150 °C with CH_4 and H_2 etchant gases to form 1.6 μm high InP nanopillars. The nanowire surfaces are smoothened by digital sidewall etching (see Supplementary Information for SEM images). We use 10 etching cycles, each comprising of a surface oxidation step and a chemical etching step to selectively remove the oxide layer.

Photoluminescence measurements. The samples were excited with a 532 nm continuous wave diode laser using a time-reversed Fourier microscope[38], giving a plane wave onto the sample with a spot radius of about 55±5 micrometer. The photoluminescence was measured using an Andor Shamrock spectrograph equipped with an Andor iDus CCD camera. The collection efficiency of the setup at the emission wavelength was determined as is described in detail in the Supplementary Information.

References

1. Yablonovitch, E. Statistical ray optics. *J. Opt. Soc. Am.* **72,** 899 (1982).
2. Campbell, P. & Green, M. A. The limiting efficiency of silicon solar cells under concentrated sunlight. *IEEE Trans. Electron Devices* **33,** 234–239 (1986).
3. Cao, L. *et al.* Engineering light absorption in semiconductor nanowire devices. *Nat. Mater.* **8,** 643–647 (2009).
4. Polman, A. & Atwater, H. A. Photonic design principles for ultrahigh-efficiency photovoltaics. *Nat. Mater.* **11,** 174–7 (2012).
5. Brongersma, M. L., Cui, Y. & Fan, S. Light management for photovoltaics using high-index nanostructures. *Nat. Mater.* **13,** 451–60 (2014).
6. Zhu, J. *et al.* Optical absorption enhancement in amorphous silicon nanowire and nanocone arrays. *Nano Lett.* **9,** 279–282 (2009).
7. Garnett, E. C. & Yang, P. Light trapping in silicon nanowire solar cells. *Nano Lett.* **10,** 1082–1087 (2010).
8. Green, M. A., Emery, K., Hishikawa, Y., Warta, W. & Dunlop, E. D. Solar cell efficiency tables (version 46). *Prog. Photovoltaics Res. Appl.* **23,** 805–812 (2015).
9. Shockley, W. & Queisser, H. J. Detailed Balance Limit of Efficiency of p-n Junction Solar Cells. *J. Appl. Phys.* **32,** 510 (1961).
10. Sandhu, S., Yu, Z. & Fan, S. Detailed balance analysis of nanophotonic solar cells. *Opt. Express* **21,** 1209–17 (2013).
11. Sandhu, S., Yu, Z. & Fan, S. Detailed Balance Analysis and Enhancement of Open-Circuit Voltage in Single-Nanowire Solar Cells. *Nano Lett.* **14,** (2014).
12. Kosten, E. D., Atwater, J. H., Parsons, J., Polman, A. & Atwater, H. A. Highly efficient GaAs solar cells by limiting light emission angle. *Light Sci. Appl.* **2,** e45 (2013).
13. Krogstrup, P. *et al.* Single-nanowire solar cells beyond the Shockley-Queisser limit. *Nat. Photonics* **7,** 306–310 (2013).
14. Würfel, P. *Physics of Solar Cells*. (WILEY-VCH Verlag, 2005).
15. Miller, O. D., Yablonovitch, E. & Kurtz, S. R. Strong Internal and External Luminescence as Solar Cells Approach the Shockley-Queisser Limit. *IEEE J. Photovoltaics* **2,** 303–311 (2012).
16. Steiner, M. A. *et al.* Effects of Internal Luminescence and Internal Optics on Voc and Jsc of III-V Solar Cells. *IEEE J. Photovoltaics* **3,** 1437–1442 (2013).
17. Ganapati, V., Steiner, M. A. & Yablonovitch, E. The Voltage Boost Enabled by Luminescence Extraction in Solar Cells. *IEEE J. Photovoltaics* **99,** 1–9 (2016).
18. Rau, U., Paetzold, U. W. & Kirchartz, T. Thermodynamics of light management in photovoltaic devices. *Phys. Rev. B* **90,** 035211 (2014).
19. Diedenhofen, S. L., Janssen, O. T. A., Grzela, G., Bakkers, E. P. A. M. & Gómez Rivas, J. Strong geometrical dependence of the absorption of light in arrays of semiconductor nanowires. *ACS Nano* **5,** 2316–2323 (2011).
20. Claudon, J. *et al.* A highly efficient single-photon source based on a quantum dot in a photonic nanowire. *Nat. Photonics* **4,** 174–177 (2010).
21. Wallentin, J. *et al.* InP Nanowire Array Solar Cell Achieving 13.8% Efficiency by Exceeding the Ray Optics Limit. *Science* **339,** 1057–1060 (2013).

22. Joyce, H. J. *et al.* Ultralow surface recombination velocity in InP nanowires probed by terahertz spectroscopy. *Nano Lett.* **12,** 5325–30 (2012).

23. Clapham, P. B. & Hutley, M. C. Reduction of Lens Reflexion by the 'Moth-Eye' Principle. *Nature* **244,** 281–282 (1973).

24. Ross, R. T. Some Thermodynamics of Photochemical Systems. *J. Chem. Phys.* **46,** 4590 (1967).

25. Würfel, P. The chemical potential of radiation. *J. Phys. C Solid State Phys.* **15,** 3967–3985 (1982).

26. Rau, U. Reciprocity relation between photovoltaic quantum efficiency and electroluminescent emission of solar cells. *Phys. Rev. B* **76,** 1–8 (2007).

27. Tran, T.-T. D. *et al.* High brightness InP micropillars grown on silicon with Fermi level splitting larger than 1 eV. *Nano Lett.* **14,** 3235–3240 (2014).

28. Schnitzer, I., Yablonovitch, E., Caneau, C. & Gmitter, T. J. Ultrahigh spontaneous emission quantum efficiency, 99.7% internally and 72% externally, from AlGaAs/GaAs/AlGaAs double heterostructures. *Appl. Phys. Lett.* **62,** 131–133 (1993).

29. Semyonov, O., Subashiev, A., Chen, Z. & Luryi, S. Radiation efficiency of heavily doped bulk n-InP semiconductor. *J. Appl. Phys.* **108,** 013101 (2010).

30. Rosenwaks, Y., Tsimberova, I., Gero, H. & Molotskii, M. Minority-carrier recombination in p-InP single crystals. *Phys. Rev. B* **68,** 115210 (2003).

31. van Dam, D. *et al.* Directional and Polarized Emission from Nanowire Arrays. *Nano Lett.* **15,** 4557–4563 (2015).

32. Oh, J., Yuan, H.-C. & Branz, H. M. An 18.2%-efficient black-silicon solar cell achieved through control of carrier recombination in nanostructures. *Nat. Nanotechnol.* **7,** 2–5 (2012).

33. Repo, P. *et al.* Effective passivation of black silicon surfaces by atomic layer deposition. *IEEE J. Photovoltaics* **3,** 90–94 (2013).

34. Joyce, H. J. *et al.* Electron Mobilities Approaching Bulk Limits in 'Surface-Free' GaAs Nanowires. *Nano Lett.* **14,** 5989–94 (2014).

35. Gao, Q. *et al.* Selective-Area Epitaxy of Pure Wurtzite InP Nanowires: High Quantum Efficiency and Room-Temperature Lasing. *Nano Lett.* **14,** 5206–5211 (2014).

36. Mariani, G., Scofield, A. C., Hung, C.-H. & Huffaker, D. L. GaAs nanopillar-array solar cells employing in situ surface passivation. *Nat. Commun.* **4,** 1497 (2013).

37. Kelzenberg, M. D. *et al.* Enhanced absorption and carrier collection in Si wire arrays for photovoltaic applications. *Nat. Mater.* **9,** 239–244 (2010).

38. Grzela, G. *et al.* Nanowire Antenna Absorption Probed with Time-Reversed Fourier Microscopy. *Nano Lett.* **14,** 3227–3234 (2014).

Acknowledgments

We would like to acknowledge Jaime Gómez Rivas for the use of the time-reversed Fourier microscope set-up of his group and Albert Polman for a careful reading of the manuscript. This work is supported by the Dutch Technology Foundation STW, which is part of the Netherlands Organization for Scientific Research (NWO), and partially funded by the Dutch Ministry of Economic Affairs. It is also supported by the long-term energy and innovation program EOS-LT, funded by the Dutch national government. This work is also part of the research program of the Foundation for Research on Matter (FOM), which is part of NWO.

Author contributions

Y.C. and P.J.v.V. fabricated the etched nanowires. D.v.D. and N.J.J.v.H. performed the PL measurements. S.A.M. and D.v.D. did the numerical modelling. All authors participated in analysing, discussing and interpreting the results. J.E.M.H., E.P.A.M.B. and E.C.G. supervised the research. D.v.D. wrote the manuscript, with valuable feedback of all authors.

Supplementary information for

Boosting solar cell photovoltage via nanophotonic engineering

Y. Cui[*1], *D. van Dam*[*], *S.A. Mann*[2], *N.J.J. van Hoof*[1], *P.J. van Veldhoven*[1], *E.C. Garnett*[2], *E.P.A.M. Bakkers*[1,3], *J.E.M. Haverkort*[2]

[*]*equal contribution*

[1]*Applied Physics, Eindhoven University of Technology, PO Box 513, 5600 MB Eindhoven, The Netherlands.*

[2]*Center for Nanophotonics, FOM Institute AMOLF, Amsterdam, The Netherlands.*

[3]*Kavli Institute of Nanoscience, Delft University of Technology, The Netherlands.*

Contents

1. External luminescence efficiency

At the open circuit voltage V_{oc} , a solar cell should not generate any current, but should only generate an output voltage. Looking from the outside to a solar cell, any solar photon absorbed by the solar cell has two options: (i) it either recombines nonradiatively with rate R_{nrad} or (ii) it contributes to external radiative recombination with rate R_{ext}. Note that we define the recombination rates per unit area. Intuitively, it is clear that a nonradiative recombination event does not contribute to an output voltage, but only heats the cell.

In the ideal case, in absence of non-radiative recombination, the open circuit voltage $V_{oc,ideal}$ is directly related to the ideal external radiative recombination rate $R_{ext,ideal}$ by

$$V_{oc,ideal} = \frac{k_B T}{q} \ln \frac{J_{SC}}{J_{0,ideal}} = \frac{k_B T}{q} \ln \frac{J_{SC}}{q R_{ext,ideal}}. \qquad \text{(eq S1)}$$

Here, q is the electron charge, k_B is Boltzmann's constant, T is the cell's temperature, $J_{0,ideal}$ the dark current in the radiative limit, and J_{SC} is the open-circuit current. Now that we know that R_{ext} is responsible for generating an output voltage and R_{nrad} as being responsible for losses, it is clear that we have to optimize the external luminescence efficiency (or, external radiative efficiency, or, external quantum yield). This quantity is defined in terms R_{ext} and R_{nrad} as $\eta_{ext} = \frac{R_{ext}}{R_{ext}+R_{nrad}}$. If the external luminescence efficiency is less than unity, it is immediately clear that the V_{oc} is reduced by

$$V_{oc} = \frac{kT}{q} \ln \left(\frac{J_{sc}/q}{R_{ext}+R_{nrad}} \right) = V_{oc,ideal} - \left| \frac{kT}{q} \ln(\eta_{ext}) \right|. \qquad \text{(eq. S2)}$$

This is equation 1 in the main text which shows the counterintuitive fact that the open circuit voltage is dependent on the light extraction from the solar cell. The importance for the V_{oc} of the external radiative recombination instead of the internal radiative recombination has recently been described in detail by Miller *et al.*[1]. They argue that in thermal equilibrium, R_{ext} is equal to the integrated flux of photons emitted by a black body at the cell's temperature T. Due to Kirchhoff's law, the emissivity is equal to the absorptivity, meaning that the emitted photon flux per unit solid angle is equal to $a(E,\theta)b(E)$, where $a(E,\theta)$ is the probability of a photon of energy E and incident angle with the substrate normal θ is absorbed in the cell. $b(E)$ is the black body's photon flux per unit area, unit time, unit energy, and unit solid angle.

Under 1 sun illumination, we are not in thermal equilibrium, and the emission spectrum intensity changes by a factor equal to the normalized product of the excited electron and hole concentrations n and p, which is np/n_i^2, where n_i is the intrinsic carrier concentration. From the law of mass action in quasi-equilibrium we know that $np=n_i^2 \exp(\mu/k_B T)$, where μ is the quasi-Fermi level splitting. From this we find that

$$R_{ext} = \exp\left(\frac{\mu}{k_B T}\right) \iint a(E,\theta) b(E)\, dE\, cos\theta d\Omega. \qquad \text{(eq S3)}$$

Here, θ is the polar angle and Ω the solid angle, seen from outside the cell.

Following Miller *et al.*, we can then relate the incident solar photon rate R_{sun} and the external radiative recombination rate R_{ext}. At open circuit, under ideal conditions, $R_{sun} = R_{ext}$. However, when nonradiative recombination is present, R_{ext} is reduced due to lost photons. In other words, the effective excitation (part leading to radiative recombination) is reduced to $R_{ext} = R_{sun}\eta_{ext}$. The other photons are lost due to nonradiative recombination. Since we know from equation S2 above that R_{ext} is directly

related to the splitting of quasi-Fermi levels μ, and that $\mu = qV_{OC}$, a decreased η_{ext} (or decreased R_{ext}) immediately leads to a penalty in V_{OC}, as suspected[1]. This provides a second derivation of equation 1 in the main text: $V_{oc} = V_{oc,ideal} - |\frac{k_B T}{q}\ln(\eta_{ext})|$.[2]

Note that we've assumed that the charge injection efficiency is unity and homogeneous over the cell. To be precise, the η_{ext} should be replaced by the LED quantum efficiency EQE_{LED} [2], defined as the volume (V) integral over the cell $EQE_{LED} = \int \eta'_{inj}(x,y,z)\eta'_{ext}(x,y,z)dV$. Here, η'_{inj} is the position-dependent charge injection efficiency, which is related to the carrier diffusion lengths and device architecture. η'_{ext} is the position-dependent external radiative efficiency, accounting for differences in the internal radiative efficiency η_{int} and P_{esc}. From now on, we will use the average values η_{ext}, η_{int} and $\overline{P_{esc}}$, for simplicity.

As we have addressed in the main text, η_{ext} can be written in terms of the *internal* luminescence efficiency η_{int} and the angle-, position- and energy-averaged photon reabsorption and escape probabilities $\overline{P_{abs}}$ and $\overline{P_{esc}}$. Here, $\overline{P_{abs}}$ is the probability for an internally emitted photon to be reabsorbed in the active region, and $\overline{P_{esc}}$ is the probability for a photon to escape from the device. This equation yields[3]:

$$\eta_{ext} = \frac{\eta_{int}\,\overline{P_{esc}}}{1 - \eta_{int}\overline{P_{abs}}} \qquad \text{(eq S4)}$$

Note that $\overline{P_{abs}} + \overline{P_{esc}} + \overline{P_{paras}} = 1$, where $\overline{P_{paras}}$ accounts for any parasitic losses in the device.[4] In Figure S1a we have displayed the V_{oc} for InP based on the equation above, in the absence of parasitic losses. Clearly, the effect of photon escape probability is equally important to the internal radiative efficiency. If $\eta_{int} < \sim 0.1$, the equation above can be simplified as

$$\eta_{ext} \approx \eta_{int}\,\overline{P_{esc}} \qquad \text{(eq S5).}$$

This is shown in Figure S1b. Note that this approximation does not hold if $\eta_{int} > 0.1$.

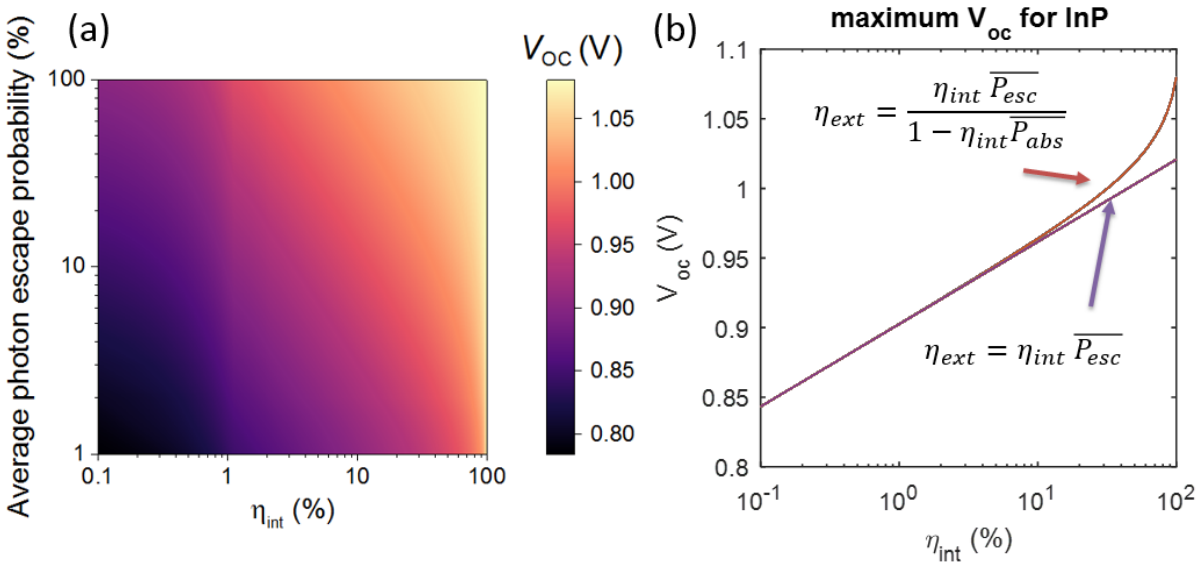

Figure S1: V_{oc} as a function of the internal radiative efficiency and photon escape probability. The calculation was performed for the AM1.5 spectrum and a band gap of 1.34 eV (e.g. InP). (a) shows a plot dependent on

both η_{int} and $\overline{P_{esc}}$. For (b) $\overline{P_{esc}}$ is fixed to 10% and the difference between the actual equation (eq1, red), and the simplified version (eq S2, purple), which is valid when η_{int}<0.1.

This dependence on the escape probability can be understood by realizing that every reabsorption event has a nonzero probability of non-radiative recombination if $\eta_{int} < 1$, such that an escaping photon is always preferred over a reabsorbed photon in order to achieve maximum η_{ext} (and therefore V_{oc}). In other words: when it is easier for photons to escape, the total number of non-radiative recombination events is reduced.

2. Fabrication of the etched nanowire array

Figure S2 (a) and (b) show the SEM pictures of the etched InP NWs before and after 10 cycles of digital sidewall etching. Without the digital etching procedure, a damaged sidewall is observed just below the SiNx masks, indicating a very rough surface. After digital etching, this damaged sidewall has been completely removed, leaving a clean and smooth NW surface.

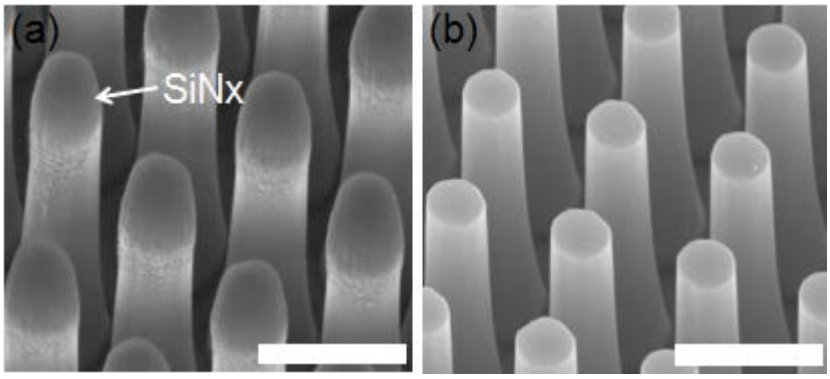

Figure S2: SEM imagines of top-down etched InP NWs before, (a), and after digital sidewall etching (b), respectively. The samples are tilted by 30°. The scale bar is 500 nm.

3. The relation between the photoluminescence intensity and the quasi-Fermi level splitting

The PL emission intensity is directly related to the splitting μ of the quasi-Fermi levels of the sample, which determines the upper limit of the V_{oc}, through the following equation[2,5,6],

$$I_{PL}(E) = a(E) I_{bb}(E) \left(\exp\left(\frac{\mu}{kT}\right) - 1\right) \quad \text{(eq S6)}$$

where E is the energy of the emission, kT is the thermal energy, equal to 25.7 meV at room temperature, $a(E)$ is the absorptivity and $I_{bb}(E)$ is the blackbody emission intensity, $I_{bb}(E) = \frac{2\pi E^2 A}{h^3 c^2} \exp\left(\frac{-E}{kT}\right)$. Here A denotes the area of the emitting region, h Planck's constant and c the speed of light. Using this equation one can find the Fermi-level splitting:

$$\mu = E + kT \ln \frac{I_{PL} h^3 c^2}{2\pi E^2 a(E) A}. \quad \text{(eq S7)}$$

μ defines the maximum value of the V_{oc} by $V_{oc,max} = \mu/q$, where q is the electron charge. A similar analysis has recently been performed by Tran *et al.*[7]

4. Absorption in nanostructured/planar material

The absorption in the nanowires has been modelled using a Finite Difference-Time Domain (FDTD) method in Lumerical inc. (Figure S3). A monochromatic plane wave is incident at normal incidence from the top of an InP nanowire array on top of an InP substrate. The electric field within the nanowire has been integrated and multiplied with the absorption coefficient. This yields an absorption of 93% at an incident wavelength of 532 nm (Figure S3). Bloch boundary conditions are used to simulate a periodic array of nanowires. For planar, semi-infinite, material, the absorption *A* equals *1-R* (*R* is the reflectance), which can be numerically calculated using Snell's law, yielding *A*=67% at 532 nm. Therefore, the absorption in the nanowire array at 532 nm is estimated to be 1.4x the absorption in planar material.

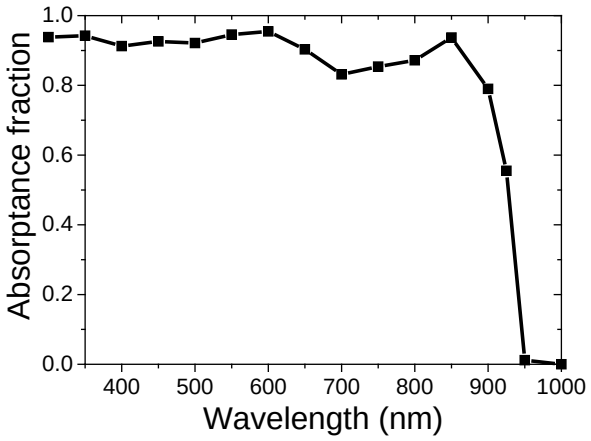

Figure S3: Simulated absorption spectrum of nanowire array as used in the measurements

5. Photon escape probabilities from nanowires and planar material

The photon escape probability of a radiative recombination event inside the nanowire array was estimated with FDTD simulations. To incorporate the effect of the array we simulated 7 by 7 unit cells, with the dipole source located in the center wire. The escape probability at a certain point $\boldsymbol{r}$ is then estimated as:

$$P_{esc}(\boldsymbol{r}) = \int_0^\infty P_{up}(E,\boldsymbol{r})S(E)dE \,/\, \int_0^\infty P_{tot}(E,\boldsymbol{r})S(E)dE \qquad \text{(eq S7)}$$

Here $P_{up}(E,r)$ is the fraction of power emitted into the upper hemisphere (free space), averaged over all dipole orientations, $P_{tot}(E,r)$ is the total power emitted by the dipoles, which may vary with position due to the modified local density of optical states. Due to the lossy nature of the material we

have to measure total power output with a small transmission box around the dipole. $S(E)$ is the van Roosbroeck-Shockley relation for emission from a semiconductor volume[3]:

$$S(E) = \frac{2\alpha(E)n^2\,E^2}{h^3c^2}\frac{1}{\exp\left(\frac{E}{k_BT}\right)-1} \qquad \text{(eq S8)}$$

Here α is the absorption coefficient, n is the real part of the refractive index, h is Planck's constant, c is the speed of light, E is the photon energy, q is the electron charge, k_B the Boltzmann constant, T is the temperature (300 K).

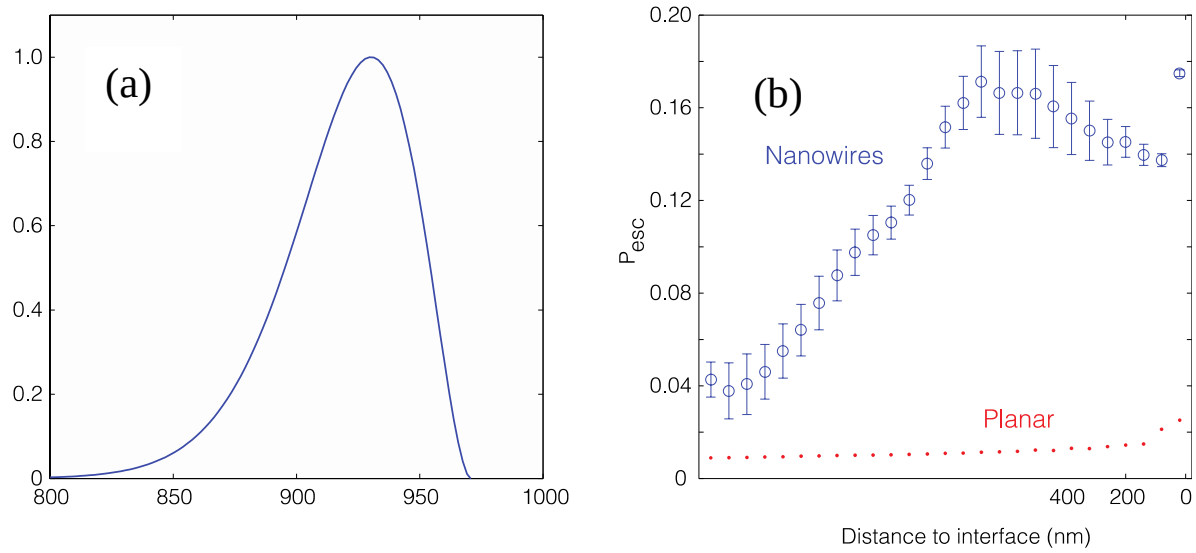

Figure S4: Simulated photon escape probability for a nanowire layer. (a) photon flux as used in the simulation. (b) Photon escape probability as a function of emitter height, for both nanowire and planar layer.

For the refractive index in this expression (α and n) we have used the FDTD data (Lumerical) such that the calculation is self-consistent. The corresponding photon flux is shown in Fig. S4a. Panel b shows the escape probability as a function of height in the nanowire, where we have averaged over multiple positions in the plane perpendicular to the nanowire axis, calculated on a grid with pixel size of 40 by 40 nm. This figure is also shown in the main text, but is added here for clarity. The error bars display the fraction of power that escapes through the sides of the simulations, and as a result it is not clear whether they eventually escape, are reabsorbed in the active layer, or in the substrate. The escape probability is as high as 16%, but varies with position, as one would expect. Determining the actual escape probability thus depends on the generation profile and carrier diffusion.

As an approximation, we use the average escape probability of dipoles located within the $1/e^2$ absorption depth of the excitation at 532 nm. Then, we find that $\overline{P_{esc}}$ for the nanowires is 13% and for the planar film is 2.1%.

6. Photoluminescence setup and calibration

The samples are excited with a plane wave in a Time-Reversed Fourier (TRF) microscope[8]. This section will explain how the setup is calibrated. This process is important for determining physical quantities such as the external luminescence efficiency and the quasi Fermi energy splitting.

We relate the illumination power (at a specific wavelength) to a number of counts in our fiber coupled spectrometer. A complete schematic overview of the setup is shown in Figure S5.

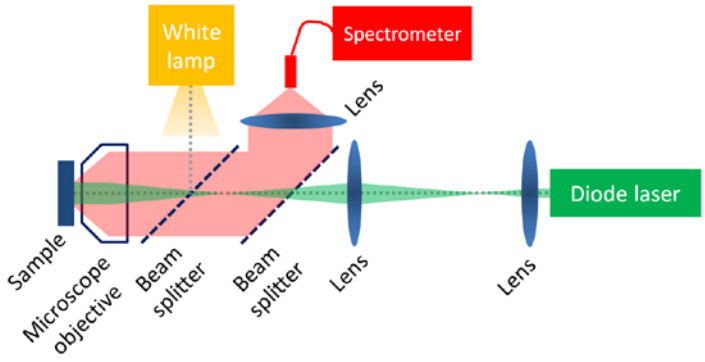

Figure S5: Schematic overview of the Time-Reversed-Fourier-Setup

First the white lamp inside the Fourier microscope is equipped with a 920 nm band pass filter with a 10 nm passband, ensuring calibration at the wavelength where our InP nanowires emit band-to-band emission. The intensity of the lamp is kept constant and its power P_{lamp} is measured at the sample position using a calibrated S121C photodiode connected to a Thorlabs power meter.

The power meter that was used to measure the illumination power is then replaced by a R=96% reflecting silver mirror and is brought into focus. This configuration represents a source of known intensity and wavelength at the sample position. This means that the number of photons $\gamma_{emitted}$ emitted per second is now known. The fraction of photons that is eventually detected in the spectrometer $\gamma_{detected}$ represents the collection efficiency of the microscope to spectrometer beam path at 920 nm. This collection efficiency is given below.

$$\eta_{setup} = \frac{\gamma_{detected}}{R\, P_{lamp}/E_{photon}} = 4.5 * 10^{-7}$$

The relative errors in the reflectance and power are much smaller than the variation in the lamp intensity and the number of detected photons, which is about 5%. Additionally, a fraction of the emission is lost since it cannot be captured by the objective. The fraction that is captured is $\frac{\int_0^{72} 2\pi\, sin\theta\, cos\theta d\theta}{\int_0^{90} 2\pi\, sin\theta\, cos\theta d\theta} = 0.90$, assuming the directional emission of nanowires and planar are not significantly different, which we verified to be a valid assumption (see Figure S6).

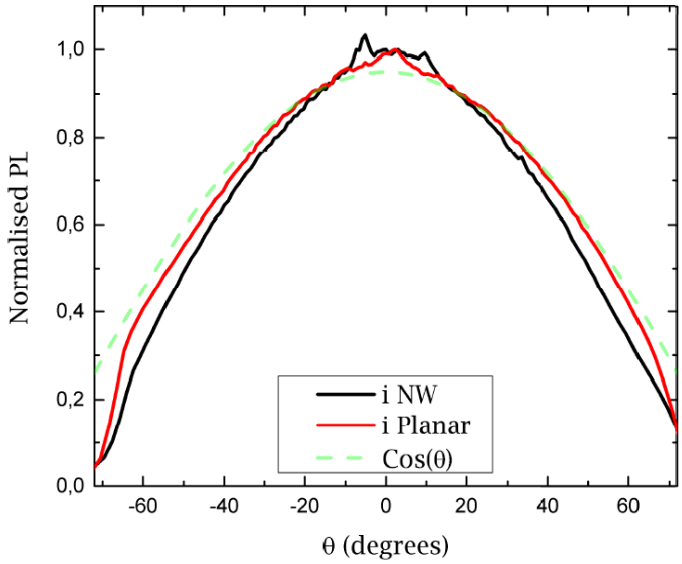

Figure S6: Unpolarized angle-dependent emission from nanowires (black) and planar (red). A cosine is shown for comparison (green, dashed). The angle-dependent emission was measured by Fourier microscopy[9].

After determining the efficiency of the setup for InP bandgap emission, an excitation power dependent measurement of both the planar and nanowire sample was conducted. A CW diode laser (532 nm) was used to excite the samples using the TRF illumination path. The laser is focused in the back focal plane of the microscope objective. This ensures that the sample is illuminated under one specific angle only, in this case straight from the top (0 degrees). This part of the setup has been described in detail elsewhere[8].

The laser power is kept constant while a set of neutral density filters (ND) was used to sweep the intensity from 1 sun to 1000 suns. These intensities are registered on the sample position with the same power meter as used before. To relate the incoming total intensity to a power density, the cross-section of the beam is imaged using a CCD camera mounted at the microscope objective position. The Gaussian plane wave coming from the TRF path is measured to have a radius of 55 ± 5 µm as it hits the sample. The PL that is generated by the sample is guided to a Andor Shamrock spectrograph equipped with a cooled CCD camera (Andor SR-303i-B) for analysis. The spectrometer collects the light coming from a disk area on the sample with a radius of 26 ± 2 µm. By comparing the overlap between the excitation spot and the PL collection area we find that 43% of the PL is occurring within the field of view. The spectra (at 1 sun) are shown in Figure 2A of the main text. As a next step the spectra are corrected for the detector efficiency and integrated over the entire spectral range of the detector to represent the total amount of photons emitted by the sample. In this way all photons are accounted for and the external luminescence efficiency in terms of the number of incoming photons versus the number of outgoing photons (i.e. the integrated PL) can be plotted, as is done in Figure 2C of the main text.

Finally the quasi Fermi energy level splitting can be determined by using the relation between absorption and spontaneous emission, as described in section 4. We take E to be the band gap energy of 1.348 eV, kT is 25.7 meV, $A = 43\% * \pi(55\ \mu\text{m})^2$ and the absorptivity at the band gap energy $a(E)$ ranges from 0.45 for planar samples up to 0.60 for NW arrays.

η_{ext} is calculated by taking the ratio of the number of photons exciting the sample and the number of emitted photons at 1 sun. It is therefore defined as $\eta_{ext} = \frac{\text{Photons emitted}}{\text{Photons absorbed}}$.

7. Comparison of internal radiative efficiency with VLS-grown InP nanowires

As a comparison for our internal radiative efficiency η_{int}; for representative VLS-grown InP nanowires, Joyce *et al*. recently reported a volume lifetime of 1.4 ns[10]. Since the radiative rate of spontaneous emission can be expressed[11] as Bnp with B=3.3*10^{-10} cm^{3}s^{-1},[12] the radiative lifetime for a background doping concentration of p=10^{15} cm^{-3} is 3.0 μs, showing that a 1.4 ns volume lifetime corresponds[11] to $\eta_{int} \approx 0.05\%$. We assume low injection level for the calculation. This value is even lower than the $\eta_{int} \approx 0.54\ \%$ of our (undoped) nanowires, showing that volume recombination is limiting the radiative efficiency of our nanowires. We also note that according to a study of Rosenwaks *et al.*[13], volume recombination is even a larger problem in p-InP due to excess nonradiative recombination due to Zn acceptors. Given this data, we have plotted the solar cell parameters corresponding to η_{int} of 1% and 90% in Fig. 4 of the main text.

8. Calculation of the open circuit voltage

Here we investigate the effect of material volume reduction and the escape probability $\overline{P_{esc}}$ on $V_{oc,ideal}$. For simplicity, we assume that surface recombination is much lower than bulk recombination, which has recently been achieved for InP nanowires[14]. Then, $J_0^{\mathrm{total}} = J_0^{\mathrm{nrad,bulk}} + J_0^{\mathrm{rad}}$. Assuming that the absorptivity stays the same, the radiative part of the dark current only depends on the total cell area, which does not change upon etching. Therefore, the reduction of the dark current in the nanostructured material is only due to the non-radiative part: $J_0^{\mathrm{nrad,nano}} = fJ_0^{\mathrm{nrad,bulk}}$, where f is the fraction of volume in the nanostructured cell relative to the planar cell ($0<f<1$). We know that $\eta_{int} = \frac{J_0^{rad}}{J_0^{rad}+J_0^{nrad}}$. The internal luminescence efficiency is modified by the material reduction, resulting in $\eta_{int}^{nano} = \frac{J_0^{rad}}{J_0^{rad}+fJ_0^{nrad,bulk}}$. Since from the expression for the internal quantum efficiency above it follows that $J_0^{nrad,bulk} = J_0^{rad}\frac{(1-\eta_{int}^{bulk})}{\eta_{int}^{bulk}}$, we find $\eta_{int}^{nano} = \frac{\eta_{int}^{bulk}}{\eta_{int}^{bulk}+f(1-\eta_{int}^{bulk})}$.

Nanostructuring does not change the dark current in the radiative limit, $V_{oc,ideal}^{nano} = V_{oc,ideal}^{bulk}$, such that $V_{oc}^{nano} \approx V_{oc,ideal}^{bulk} + \frac{kT}{q}\ln(\eta_{ext})$. For the ideal $V_{oc,ideal}^{bulk}$ we use the Shockley-Queisser voltage for a band gap of 1.34 eV, which is 1.08 V. Furthermore, in the absence of parasitic losses $\eta_{ext} = \frac{\eta_{int}\overline{P_{esc}}}{1-\eta_{int}(\overline{P_{abs}})} = \frac{\eta_{int}\overline{P_{esc}}}{1-\eta_{int}(1-\overline{P_{esc}})}$. We thus finally obtain, $V_{oc}^{nano} = V_{oc,ideal}^{bulk} + \frac{kT}{q}\ln\left(\frac{\eta_{int}^{nano}\overline{P_{esc}}}{1-\eta_{int}^{nano}(1-\overline{P_{esc}})}\right)$.

References

1. Miller, O. D., Yablonovitch, E. & Kurtz, S. R. Strong Internal and External Luminescence as Solar Cells Approach the Shockley-Queisser Limit. *IEEE J. Photovoltaics* **2,** 303–311 (2012).
2. Rau, U. Reciprocity relation between photovoltaic quantum efficiency and electroluminescent emission of solar cells. *Phys. Rev. B* **76,** 1–8 (2007).
3. Steiner, M. A. *et al.* Optical enhancement of the open-circuit voltage in high quality GaAs solar cells. *J. Appl. Phys.* **113,** 123109 (2013).
4. Rau, U., Paetzold, U. W. & Kirchartz, T. Thermodynamics of light management in photovoltaic devices. *Phys. Rev. B* **90,** 035211 (2014).
5. Ross, R. T. Some Thermodynamics of Photochemical Systems. *J. Chem. Phys.* **46,** 4590 (1967).
6. Würfel, P. The chemical potential of radiation. *J. Phys. C Solid State Phys.* **15,** 3967–3985 (1982).
7. Tran, T.-T. D. *et al.* High brightness InP micropillars grown on silicon with Fermi level splitting larger than 1 eV. *Nano Lett.* **14,** 3235–3240 (2014).
8. Grzela, G. *et al.* Nanowire Antenna Absorption Probed with Time-Reversed Fourier Microscopy. *Nano Lett.* **14,** 3227–3234 (2014).
9. Grzela, G. *et al.* Nanowire Antenna Emission. *Nano Lett.* **12,** 5481–5486 (2012).
10. Joyce, H. J. *et al.* Ultralow surface recombination velocity in InP nanowires probed by terahertz spectroscopy. *Nano Lett.* **12,** 5325–30 (2012).
11. Schnitzer, I., Yablonovitch, E., Caneau, C. & Gmitter, T. J. Ultrahigh spontaneous emission quantum efficiency, 99.7% internally and 72% externally, from AlGaAs/GaAs/AlGaAs double heterostructures. *Appl. Phys. Lett.* **62,** 131–133 (1993).
12. Ahrenkiel, R. K., Dunlavy, D. J. & Hanak, T. Minority-carrier lifetime in ITO/InP heterojunctions. *J. Appl. Phys.* **64,** 1916–1921 (1988).
13. Rosenwaks, Y., Tsimberova, I., Gero, H. & Molotskii, M. Minority-carrier recombination in p-InP single crystals. *Phys. Rev. B* **68,** 115210 (2003).
14. Gao, Q. *et al.* Selective-Area Epitaxy of Pure Wurtzite InP Nanowires: High Quantum Efficiency and Room-Temperature Lasing. *Nano Lett.* **14,** 5206–5211 (2014).